

*promoting access to White Rose research papers*



**Universities of Leeds, Sheffield and York**  
**<http://eprints.whiterose.ac.uk/>**

---

This is an author produced version of a paper published in **Physics Letters A**.

White Rose Research Online URL for this paper:  
<http://eprints.whiterose.ac.uk/4728/>

---

**Published paper**

Sreenivasan, B. (2008) *A buoyant flow structure in a magnetic field: Quasi-steady states and linear-nonlinear transitions*, Physics Letters A, Volume 372 (33), 5471 - 5478.

---

# A buoyant flow structure in a magnetic field: quasi-steady states and linear–nonlinear transitions

Binod Sreenivasan

*School of Earth and Environment, University of Leeds, Leeds LS2 9JT, United Kingdom.*

The confined evolution of a buoyant blob of fluid subject to a vertical magnetic field is investigated in the limit of low magnetic Reynolds number. When the applied magnetic field is strong, the rise velocity of the blob is small. As the vorticity diffuses along the magnetic field lines, a quasi-steady state characterised by a balance between the work done by buoyancy and Ohmic dissipation is eventually reached at time  $t_{qs} \sim (L^2/\delta^2)\tau$ , where  $L$  is the axial dimension of the fluid domain,  $\delta$  is the radius of the buoyant blob and  $\tau$  is the magnetic damping time. However, when the applied magnetic field is weak or the axial length is sufficiently large compared to the blob size, the growth of axial velocity eventually makes the advection of vorticity significant. The typical time for the attainment of this nonlinear phase is  $t_{nl} \sim N_0^{2/3}\tau$ , where  $N_0$  is the magnetic interaction parameter at time  $t = \tau$ . The order-of-magnitude estimates for the timescales  $t_{qs}$  and  $t_{nl}$  are verified by computational experiments that capture both the linear and nonlinear phases.

# 1 Introduction

In liquid metal magnetohydrodynamics (MHD), magnetic fields are used to suppress motions in an electrically conducting fluid. Common examples of this effect are the role of a static magnetic field in the delayed onset of Rayleigh-Bénard convection in a fluid heated from below [1] and the damping of free-surface waves by a vertical magnetic field [2, 3]. As fluid flows are typically made up of an ensemble of localized eddies or buoyant plumes, several previous studies focussed on these flow structures and thereby obtained considerable insight into the behaviour of large scale flows. The spatio-temporal evolution of isolated vortices subject to static magnetic fields has been studied extensively in [4, 5, 6]. Axisymmetric buoyant fluid blobs in a quiescent fluid were investigated for the occurrence (or absence) of finite-time singularities in the “vortex sheets” that form at their fronts [7, 8]. The presence of a strong, ambient magnetic field affects the evolution of a blob by inhibiting the formation of this vortex sheet [9]. In an infinite domain, however, the magnetic field does not affect the vertical momentum of the blob, which increases linearly with time. The evolution of buoyant blobs in a liquid metal may have implications for the Earth’s dynamo. Isolated blobs of material are thought to be released from the mushy zone near the Earth’s inner core boundary, each blob driving a Taylor column [10]. The dynamics of such buoyant parcels under the combined influence of a toroidal magnetic field and background rotation have been analysed in a geophysical context [11]. In this paper I look at buoyant blobs in a confined fluid, where the dynamics are controlled by both the strength of the ambient magnetic field and the size of the domain. Under a strong magnetic field, the evolution is linear, in the sense that the diffusion of vorticity along the magnetic field lines dominates over nonlinear advection. Eventually, a quasi-steady state, produced by a balance between the work done by buoyancy and

Ohmic dissipation of the flow, is reached. On the other hand, if the magnetic field is weak or the fluid domain is large, the above linear phase is followed by a phase wherein non-linear advection becomes significant. The timescale for this linear–nonlinear transition is estimated from an order-of-magnitude analysis and verified independently by numerical simulations.

This paper is organized as follows. In Section 2, the governing equations for the problem and their interpretation are presented. In Section 3, the model problem is described and the timescales of occurrence of the quasi-steady and nonlinear phases are derived. Comparisons with the infinite-domain problem and previous analogous studies on MHD vortices are made where appropriate. Section 4 is devoted to a computational study of a buoyant blob in a cavity and comparison of the results with the estimates obtained in Section 3. The main results are summarized in Section 5.

## 2 Governing equations

We consider the evolution of a localized density disturbance in an inviscid, incompressible, Boussinesq fluid. The fluid has a density perturbation  $\delta\rho$ , which is essentially  $\delta\rho = -\rho\alpha T$ , where  $\alpha$  is the coefficient of thermal expansion ( $\text{K}^{-1}$ ) and  $T$  is the temperature relative to the value at infinity, associated with the density variation. The fluid is penetrated by a vertical, uniform magnetic field,  $B\hat{\mathbf{e}}_z$ . The magnetic Reynolds number [12], defined as the ratio of the magnetic diffusion time,  $l^2/\eta$ , to the the eddy turn-over time,  $l/u$ , is small. (Here  $l$  and  $u$  are typical length and velocity scales and  $\eta$  is the magnetic diffusivity). The condition

$$R_m = \frac{ul}{\eta} \ll 1$$

is usually satisfied in laboratory hydromagnetics. In the Earth’s liquid iron outer core of size  $l = 2200$  km,  $R_m$  is of order  $10^2$ . However, isolated vortex “blobs” of  $l \sim 6$  km would still have  $R_m \sim 1$ , if we assume  $u = 3 \times 10^{-4}$  ms $^{-1}$  and  $\eta = 2$  m $^2$ s $^{-1}$ . The assumption of low  $R_m$  is useful in vortex dynamics because the back-reaction of the velocity field on the magnetic field can be neglected. In other words, the locally induced magnetic field is small relative to the global, ambient field.

The initial configuration of the buoyant blob is shown in figure 1 (a). The blob has a maximum temperature  $T_0$  at its centre. We restrict our analysis to axisymmetric motion in cylindrical polar coordinates  $(r, \theta, z)$ , with the gravitational acceleration  $g$  aligned with the  $z$ -direction. The temperature distribution creates a poloidal velocity field  $\mathbf{u}$  that causes the blob to rise against gravity. The electromagnetic forces, on the other hand, tend to suppress this motion. The governing equation of motion is,

$$\frac{D\mathbf{u}}{Dt} = -\nabla\left(\frac{p}{\rho}\right) + g\alpha T\hat{\mathbf{e}}_z + \mathbf{j} \times \mathbf{B}/\rho, \quad (1)$$

where  $p$  is the fluid pressure,  $D/Dt$  is the total derivative, and  $\mathbf{j}$  is the electric current density. For small  $R_m$ , Ohm’s law has the form [1]

$$\mathbf{j} = \sigma(-\nabla\phi + \mathbf{u} \times \mathbf{B}), \quad (2)$$

where  $\phi$  is the electric potential and  $\sigma$  is the electrical conductivity. Now, the poloidal velocity field  $\mathbf{u}$  interacts with  $\mathbf{B}$  to produce electric currents that are purely azimuthal. These current lines automatically form closed loops without the need for a net induced electric potential gradient. Hence, the induced current is,

$$\mathbf{j}_\theta = -\sigma u_r B \hat{\mathbf{e}}_\theta,$$

and the “braking” Lorentz force is given by [9],

$$\mathbf{F}_p = \mathbf{j}_\theta \times \mathbf{B}/\rho = -\frac{u_r}{\tau} \hat{\mathbf{e}}_r, \quad (3)$$

where  $\tau = \rho/\sigma B^2$  is the typical electromagnetic damping time, also known as the Joule time. Thus the governing equations of our problem are,

$$\frac{DT}{Dt} = 0; \quad (4)$$

$$\frac{D\mathbf{u}}{Dt} = -\nabla\left(\frac{p}{\rho}\right) + g\alpha T\hat{\mathbf{e}}_z - \frac{u_r}{\tau}\hat{\mathbf{e}}_r, \quad (5)$$

where we have neglected thermal diffusion. Although turbulent diffusion of momentum and heat cannot be ignored either in a laboratory MHD experiment or in the Earth's liquid iron core [11], here we assume that these are small compared to magnetic diffusion over the localized volume of a fluid blob.

The curl of equation (5) gives the vorticity equation:

$$\frac{D}{Dt}\left(\frac{\omega_\theta}{r}\right) = -\frac{1}{r}\left(g\alpha\frac{\partial T}{\partial r} + \frac{1}{\tau}\frac{\partial u_r}{\partial z}\right). \quad (6)$$

The growth of the azimuthal vorticity,  $\omega_\theta$  is fed by  $\partial T/\partial r$ , the process being checked by the electromagnetic forces. The dissipative effect of the magnetic field may be understood from the energy equation, obtained by taking the dot product of (5) with  $\mathbf{u}$  and integrating the result over the fluid volume:

$$\frac{d}{dt}\int\left(\frac{u^2}{2}\right)dV = \int g\alpha T u_z dV - \frac{1}{\tau}\int u_r^2 dV. \quad (7)$$

The first term on the right hand side of (7) is the rate of working of the buoyancy force (usually, but not always positive) and the second term corresponds to Ohmic dissipation of the flow. Now, using (4) we may write,

$$g\alpha T u_z = \frac{D}{Dt}[g\alpha T z].$$

Thus the energy equation may be re-written as,

$$\frac{d}{dt}\left[\underbrace{\int\left(\frac{u^2}{2}\right)dV}_{\text{KE}} + \underbrace{\int g\frac{\delta\rho}{\rho} z dV}_{\text{PE}}\right] = \frac{1}{\tau}\int u_r^2 dV. \quad (8)$$

As the blob rises, the kinetic energy (KE) grows at the expense of the potential energy (PE), but the total energy falls as a result of Ohmic dissipation.

For axisymmetric motion, the poloidal velocity field  $\mathbf{u}$  in (5) may be expressed in terms of a streamfunction,  $\psi$  in cylindrical polar coordinates:

$$\mathbf{u} = (u_r, 0, u_z) = \left( -\frac{1}{r} \frac{\partial \psi}{\partial z}, 0, \frac{1}{r} \frac{\partial \psi}{\partial r} \right),$$

so that, the azimuthal vorticity,  $\omega_\theta$ , and  $\psi$  are related by [7],

$$r\omega_\theta = -\left[ \frac{\partial^2 \psi}{\partial z^2} + r \frac{\partial}{\partial r} \left( \frac{1}{r} \frac{\partial \psi}{\partial r} \right) \right] = -\nabla_\star^2 \psi. \quad (9)$$

Hence, (6) may be recast as an equation in  $\psi$  as follows:

$$\frac{D}{Dt} \nabla_\star^2 \psi = r \frac{\partial}{\partial r} (g\alpha T) - \frac{1}{\tau} \frac{\partial^2 \psi}{\partial z^2}. \quad (10)$$

The second term on the right hand side of (10) represents diffusion of streamlines along the magnetic field lines, which competes with the generation of the poloidal flow by temperature gradients, given by the first term on the right.

In the next section, the evolution of a blob in a confined domain is discussed. Comparisons with the results for an infinite domain are made where appropriate.

### 3 The model problem

Our model problem is shown schematically in figure 1(b). The buoyant parcel is located at the centre of a tall cylindrical cavity containing quiescent, electrically conducting fluid. The initial temperature distribution is

$$T = T_0 \exp\left[-\left(r^2 + (z - L/2)^2\right)/\delta^2\right], \quad (11)$$

where  $T_0$  is the maximum temperature at the centre of the disturbance,  $L$  is the length of the cavity,  $R$  is its radius and  $\delta$  is the decay lengthscale of the temperature perturbation. We choose  $L \gg \delta$ , so that the dynamics of the blob can be studied for a long period of time before boundary effects come into play. As the blob rises, the generated flow is marked by streamlines which have the closed pattern shown in figure 1(b). As we shall see in Section 4, the choice of the above cylindrical geometry admits a simple spectral solution of the model problem, while not affecting the generality of the analysis.

### 3.1 Integrals of vorticity and momentum

Integrating (6) over the entire volume yields

$$\frac{d}{dt} \int \left( \frac{\omega_\theta}{r} \right) dV = 2\pi \int_0^L g\alpha T(r=0, z) dz - \frac{2\pi}{\tau} \int_0^R [(u_r)_T - (u_r)_B] dr, \quad (12)$$

where the subscripts  $T$  and  $B$  represent the top and bottom of the cavity. Note that second term on the right side of (12) is positive for a rising blob, as the radial velocity of the fluid is higher at the top than at the bottom. Hence, the growth of  $\omega_\theta/r$  with time is not monotonic as for an infinite domain [9], but restricted by the imposed magnetic field. The linear momentum of the flow, given by [13]

$$\mathbf{L} = \frac{1}{2} \int (\mathbf{x} \times \boldsymbol{\omega}) dV$$

has the only non-zero component  $L_z = \frac{1}{2} \int r\omega_\theta dV$ . The evolution of linear momentum may thus be written as follows:

$$\frac{DL_z}{Dt} = \frac{D}{Dt} \left( \frac{1}{2} r\omega_\theta \right) = -\frac{1}{2} r \left[ \frac{\partial}{\partial r} (g\alpha T) + \frac{1}{\tau} \frac{\partial u_r}{\partial z} \right] + u_r \omega_\theta.$$

Substituting for  $\omega_\theta = (\partial u_r/\partial z - \partial u_z/\partial r)$ , invoking the continuity equation, and after some manipulation, we obtain

$$\frac{D}{Dt}\left(\frac{1}{2}r\omega_\theta\right) = g\alpha T - \frac{1}{2r}\frac{\partial}{\partial r}(r^2g\alpha T) - \frac{r}{2\tau}\frac{\partial u_r}{\partial z} + \frac{\partial}{\partial z}\left(\frac{u_r^2}{2} - \frac{u_z^2}{2}\right) - \frac{1}{r}\frac{\partial}{\partial r}(ru_ru_z). \quad (13)$$

Integrating (13) over the entire volume then yields,

$$\frac{d}{dt}\int\left(\frac{1}{2}r\omega_\theta\right)dV = \int g\alpha T dV - \frac{\pi}{\tau}\int_0^R r^2[(u_r)_T - (u_r)_B] dr + \pi\int_0^R r[(u_r^2)_T - (u_r^2)_B] dr, \quad (14)$$

as the remaining terms vanish. The first term on the right hand side of (14) is an invariant as temperature is materially conserved by way of (4). Under a magnetic field, the second term on the right side of (14) could be significant and of the same order as the first term, cancelling out the temperature integral. The third term on the right is usually small as it involves squares of radial velocities of opposite sign but comparable magnitudes. For an infinite domain, both the second and third terms on the right hand side of (14) vanish and hence the vertical momentum increases linearly with time, unaffected by the magnetic field.

### 3.2 Long-time behaviour in a strong magnetic field: a quasi-steady state

It is common to express the strength of the applied magnetic field in terms of a dimensionless number, the magnetic interaction parameter, defined as the ratio of the eddy turn-over time to the Joule time [1]:

$$N = \frac{l/u}{\tau} = \frac{\sigma B^2 \delta}{\rho u}. \quad (15)$$

In classical hydrodynamics, the velocity of a buoyant fluid blob is commonly estimated by  $u \sim (g\alpha T_0 \delta)^{1/2}$ , from a balance between the buoyancy and nonlinear inertial forces in the

equation of motion. However, in the presence of a strong magnetic field, nonlinear inertia is negligible in comparison with the Lorentz force and so the magnetic field determines the fluid velocity from time  $t \sim \tau$ . The radial velocity at  $t \sim \tau$  is estimated from (5) as

$$u_r \sim g\alpha T_0 \tau.$$

Thus, the interaction parameter at  $t \sim \tau$  is given by

$$N_0 = \frac{\delta}{g\alpha T_0 \tau^2}. \quad (16)$$

For times  $t > \tau$ , the flow diffuses along the magnetic field lines, and the dominant component of the velocity would be the vertical ( $z$ ) component, estimated by

$$u_z \sim g\alpha T_0 \tau \frac{l_{\parallel}}{\delta}, \quad (17)$$

where  $l_{\parallel}$  is the lengthscale parallel to  $\mathbf{B}$ . The maximum vertical velocity of the parcel in a cavity of length  $L$  would thus be of order  $g\alpha T_0 \tau L/\delta$ . Note, however, that if the magnetic field is strong,  $\tau$  is small, and so is  $u_z$ . This implies that the advection of the temperature field is small and the blob is hardly displaced from its initial position at the centre of the cavity in figure 1(b).

To obtain the long-time behaviour of the blob, we consider (6) in the limit of large  $N$ :

$$\frac{\partial \omega_{\theta}}{\partial t} = -g\alpha \frac{\partial T}{\partial r} - \frac{1}{r\tau} \frac{\partial^2}{\partial z^2} [\nabla_{\star}^{-2}(r\omega_{\theta})], \quad (18)$$

where  $\nabla_{\star}^{-2}$  is the inverse of the special Laplacian operator in (9). An order-of-magnitude estimate of the electromagnetic force on the right hand side of (18) gives

$$\frac{\partial \omega_{\theta}}{\partial t} \sim -g\alpha \frac{\partial T}{\partial r} + \frac{\delta^2}{\tau} \frac{\partial^2 \omega_{\theta}}{\partial z^2}. \quad (19)$$

The vorticity thus propagates along the  $\mathbf{z}$ -coordinate with a *pseudo-diffusivity*  $\delta^2/\tau$ . (Compare this with the analogous problem of two-dimensionalization of an MHD turbulent flow [14]). It is evident from (19) that, for a confined domain of length  $L$ , a quasi-steady state is attained for

$$t = t_{qs} \gtrsim \left(\frac{L^2}{\delta^2}\right)\tau. \quad (20)$$

Under this steady-state condition, equation (6) reduces to

$$g\alpha\frac{\partial T}{\partial r} + \frac{1}{\tau}\frac{\partial u_r}{\partial z} = 0. \quad (21)$$

The regime given by (21) presents a few interesting features that serve as diagnostics for high  $N$  (a strong magnetic field). Since the temperature distribution at any time may be assumed to be identical to that at  $t = 0$ , i.e. (11), the temperature gradients in (21) are confined to the sections  $z_1$  and  $z_2$  that enclose the blob (see figure 2). The values of  $z_1$  and  $z_2$  are determined by the decay length of the perturbation,  $\delta$ . It follows that the radial velocity,  $u_r$ , in the outer region shown hatched in figure 2 is independent of  $z$ . Also, by virtue of the symmetry of the temperature distribution about the  $z = L/2$  plane,  $u_r$  at any section in the upper half of the cylindrical domain is equal and opposite to its value at the section equidistant from the mid-plane in the lower half. Integrating (21) over  $z$  between limits  $z_1$  and  $z_2$ , we obtain,

$$V(r) = \frac{\tau}{2} \int_{z_1}^{z_2} g\alpha \frac{\partial T}{\partial r} dz. \quad (22)$$

Thus, the streamfunction,  $\psi$ , is given by

$$\psi(r, z) = rV(r)(L - z). \quad (23)$$

Further, from (12) and (14), we obtain,

$$\int_0^R u_r dr = \frac{1}{2} g \alpha \tau \int_0^L T(r=0, z) dz; \quad (24)$$

$$\int_0^R r^2 u_r dr = \frac{\tau g \alpha}{2\pi} \int T dV. \quad (25)$$

The left hand side integrals in (24) and (25) may be evaluated for any  $z$  in the range  $z_2 < z < L$ .

### 3.3 A nonlinear regime

Let us now consider a buoyant blob of fluid evolving either (a) in a moderate/weak magnetic field or (b) in a strong magnetic field but in a domain whose axial length is considerably larger than the lengthscale of the density perturbation. We shall assume that the Lorentz force is dominant at  $t \sim \tau$ , so that the initial evolution is linear and governed by (18). However, the vertical velocity, given by (17), also becomes significant as time progresses. As the convective turn-over time becomes shorter, the nonlinear inertial forces in the momentum equation increase in magnitude and eventually become comparable to the Lorentz force. The evolution of the blob then ceases to be linear. As both the Lorentz and inertial forces are generally rotational, the relative magnitudes of the two forces are estimated by

$$N_t = \frac{\nabla \times (\mathbf{j} \times \mathbf{B})}{\nabla \times (\mathbf{u} \cdot \nabla \mathbf{u})} \sim \frac{\delta/u_z}{\tau} \left( \frac{\delta}{l_{\parallel}} \right)^2, \quad (26)$$

where  $N_t$  is the *true* value of the interaction parameter. Since (19) suggests that the diffusive lengthscale,  $l_{\parallel}$  grows as  $\sim \delta(t/\tau)^{1/2}$  in the initial linear phase, and the transverse lengthscale  $\delta$  is unaffected by the magnetic field, (26) is readily simplified as

$$N_t \sim N_0 (t/\tau)^{-3/2}, \quad (27)$$

where  $N_0$  is the interaction parameter at  $t = \tau$ . In other words,  $N_t$  decreases continuously from its value at  $t = \tau$ , and when  $t = t_{nl} \sim N_0^{2/3}\tau$ , a nonlinear phase of evolution is reached. As the Lorentz force, given by (3), remains approximately constant, further ‘free’ evolution of the blob (i.e. unaffected by the boundaries) would lead to a dominance of the inertial forces. This strongly nonlinear regime where  $N_t < 1$  is marked by advection of the temperature and vorticity fields, causing the blob to deform into the well-known mushroom-like structure with steep gradients at its front [8].

It is worth comparing the linear–nonlinear transition of a buoyant blob with an equivalent transition in the analogous problem of a freely-decaying vortex under a magnetic field [5, 6]. Consider an isolated fluid vortex of radius  $\delta$  with its axis aligned with a strong, uniform magnetic field  $\mathbf{B}$  at  $t = 0$ . While the flow diffuses along the magnetic field lines, the convective turn-over time  $\delta/u$  increases because the kinetic energy falls by Ohmic dissipation. However, the electric current density also falls significantly during this phase as the axial currents have to travel through longer paths, as evident from the curl of Ohm’s law:

$$\nabla \times \mathbf{j} = \sigma(\mathbf{B} \cdot \nabla)\mathbf{u} \sim \sigma B u / l_{\parallel},$$

where  $\sigma$  is the conductivity of the fluid and  $l_{\parallel}$  is the lengthscale parallel to the magnetic field direction. The rate of fall of the Lorentz forces is greater than the rate of fall of the inertial forces, and eventually, the evolution enters a nonlinear phase wherein the two forces are of the same of magnitude. Sreenivasan & Alboussière [5] found that the interaction parameter for this case varies as

$$N_t \sim N_0(t/\tau)^{-1/2},$$

where  $N_0$  here is the interaction parameter at  $t = 0$ . When  $t = t_{nl} \sim N_0^2\tau$ , the flow becomes nonlinear.

In summary, the evolution of a buoyant blob in a given magnetic field is influenced by two timescales – one for the attainment of a quasi-steady state,  $t_{qs}$ ; and one for the onset of nonlinear evolution,  $t_{nl}$ . The long-time structure of the buoyant fluid blob would be determined by whether  $t_{qs}$  is less or greater than  $t_{nl}$ .

## 4 Computational experiments

In this section, the evolution of a localized buoyant parcel of fluid contained in a finite domain is studied numerically. The basic configuration is as in figure 1 (b), where the initial axisymmetric temperature distribution of characteristic lengthscale  $\delta$ , given by (11), is located at the centre of a cylindrical cavity of length  $L = 20\delta$  and radius  $R = 5\delta$ . Equations (4) and (5) are solved for the above initial condition. The blob radius is chosen as 0.01 units, and the constant  $g\alpha T_0$  is chosen to be 0.012, corresponding to values of  $g = 10 \text{ ms}^{-2}$ ,  $\alpha = 6 \times 10^{-5}$  and  $T_0 = 20^\circ\text{C}$ . The temperature  $T$  is expanded as the following Fourier-Bessel series:

$$T = \sum_{m,n} \hat{T}_{mn} J_0(\epsilon_n r/R) \sin(m\pi z/L), \quad (28)$$

where  $\epsilon_n$  are the roots of  $J_0(x)$ . The temperature is zero at the boundaries, so the maximum temperature difference,  $T_0$ , drives a confined, axisymmetric poloidal velocity field given by the streamfunction,

$$\psi = \sum_{m,n} \hat{\psi}_{mn} \frac{r}{R} J_1(\epsilon_n r/R) \sin(m\pi z/L). \quad (29)$$

The numerical method involves time-stepping the spectral coefficients  $\hat{T}$  and  $\hat{\psi}$  and recovering the temperature and streamfunction using the inverse transformations of (28)

and (29), quite similar to that used for the analogous problem of a swirling vortex in a confined domain [5]. The induced electric currents do not need a boundary condition as they are purely azimuthal. As temperature should be materially conserved by (4), the maximum temperature is tracked during the simulation to check for accuracy. When the maximum temperature falls by 0.5% of its value at  $t = 0$ , the simulation is stopped.

The magnetic field strength is determined by the value of  $\tau$  in the model. All calculations are performed for an interaction parameter,  $N_0 \gg 1$ , where  $N_0$  is defined at  $t = \tau$  by (16). At this stage, the Lorentz force is dominant, and the turn-over time  $\delta/u$  is controlled by the magnetic field, via (17). From the scaling for  $u_z$ , the kinetic energy of the flow is scaled based on its terminal value in this ‘linear’ phase:

$$E = \frac{1}{2} \int u^2 dV \sim (g\alpha T_0 \tau)^2 L^3. \quad (30)$$

Secondly, since the axial location of the blob,  $z_f$  is related to  $u_z$  by  $dz_f/dt = u_z$ , we obtain

$$z_f \sim g\alpha T_0 \tau^2 L/\delta. \quad (31)$$

Finally, the global linear momentum,  $L$ , scales as

$$L = \frac{1}{2} \int r\omega_\theta dV \sim g\alpha T_0 \tau L^2 \delta. \quad (32)$$

Figure 3 (a) shows the evolution of the global kinetic energy density,  $\frac{1}{2}u^2$ . The stronger the magnetic field (the smaller the value of  $\tau$ ), the smaller the energy released to the poloidal flow. When the energy is normalized by the scaling in (30), the curves collapse into one, indicating a self-similar behaviour in the linear phase of evolution [figure 3 (b)]. The kinetic energy for  $N_0 = 8.35 \times 10^5$  ( $\tau = 10^{-3}$ ; case 1 in Table 1) saturates into a quasi-steady state, showing that the work done by buoyancy is absorbed entirely by

Ohmic dissipation in equation (7). Although the estimate (20) predicts a steady state for  $t > 400\tau$  for this geometry ( $L = 20\delta$ ), we find a gradual transition to this state up to  $t \sim 1500\tau$ . The energies for  $N_0 = 5.208 \times 10^4$  and 8333.3 (cases 2 & 3) depart from self-similar behaviour at  $t \approx 1000\tau$  and  $t \approx 300\tau$  respectively, suggesting that the scaling (17), valid for  $N \gg 1$ , breaks down at these times. Now, the onset of nonlinear evolution, described in Section 3.3, is expected to happen when  $t = t_{nl} \sim N_0^{2/3}\tau$ . A comparison of the value of  $t_{nl}$  in the computations with this theoretical estimate is given in Table 1, cases 2–4. The ratio of the two times is of order unity.

It is evident from the computations that the evolution of the buoyant blob depends entirely on the relative magnitudes of the timescales for attainment of the nonlinear and quasi-steady states,  $t_{nl}$  and  $t_{qs}$ . In cases 2–4 in Table 1,  $t_{nl}$  is either of the same order of magnitude as, or significantly smaller than,  $t_{qs}$  ( $t_{qs} \sim 1500\tau$  in the computation). Hence, the advection of temperature (and vorticity) becomes significant. For the strongest magnetic field ( $N_0 = 8.33 \times 10^5$ ; case 1), on the other hand, the theoretical estimate of the linear–nonlinear transition time gives  $t_{nl} \sim 8854\tau$ . This timescale being significantly larger than  $t_{qs}$ , the evolution never becomes nonlinear, but becomes quasi-steady when the flow diffuses over the entire axial length of the domain (also see figure 7 below). A cavity with axial dimension  $L \gtrsim 50\delta$  would be required to force a nonlinear regime in this case. To test the competition between the timescales  $t_{qs}$  and  $t_{nl}$  in the problem, two runs were performed for  $N_0 = 8333.3$  (see case 3), but in shorter cavities of  $L = 8\delta$  and  $5\delta$ . The kinetic energy readily enters a steady state from an initial linear phase when  $L = 5\delta$  because  $t_{qs} < t_{nl}$  for this geometry (figure 4). For  $L = 8\delta$ , the kinetic energy departs from the steady state at  $t \sim 300\tau$ , the timescale for nonlinear transition.

Figure 5 gives the vertical displacement of the blob as a function of time, obtained by

tracking the axial location of the maximum temperature during the calculation. From figure 5 (a) it is evident that the motion of the blob is severely restricted by a strong magnetic field. The curves of normalized displacement in figure 5 (b) confirm the scaling for  $N \gg 1$  but are less sensitive to the onset of nonlinear inertia. From the curves of global linear momentum in figure 6, we find that the initial growth of momentum is cancelled out by the magnetic field acting at  $t \sim \tau$  via equation (14). Again, a quasi-steady state is reached for  $N_0 = 8.33 \times 10^5$  and self-similarity holds with the scaling in (32).

The structures of the temperature field and flow, given in figures 7–9 support our earlier findings. Figure 7 shows the vorticity diffusing along the magnetic field lines, for  $N_0 = 8.33 \times 10^5$  (case 1, Table 1). At  $t \sim 500\tau$ , a *quasi-two-dimensional* state is reached where the lines of vorticity fill the entire domain. This evolution is consistent with the  $(t/\tau)^{1/2}$  growth of the parallel lengthscale. From figure 8, we note that the initial temperature distribution is preserved throughout the simulation, pointing to negligible advection of temperature for this case. The streamlines are spread out in radius during the initial phase of growth of  $\psi$ , but are eventually confined to a thin cylindrical region that circumscribes the density perturbation, where the radial temperature gradient is appreciable (note from (10) that the structure of  $\partial T/\partial r$  determines the structure of  $\psi$  when  $D/Dt = 0$ ). For  $N_0 = 5.208 \times 10^4$ , the temperature and vorticity fields undergo some distortion within  $t \sim 1000\tau$ , indicating that the advection of these fields is not small. For  $N_0 = 8333.3$  (figure 9), this distortion is appreciable for  $t > 350\tau$ . The blob develops steep gradients at the front and an indentation at its base.

We finally return to the quasi-steady solution of case 1 ( $N_0 = 8.33 \times 10^5$ ), which presents some interesting features as noted in Section 3.2. Figure 10 shows the radial velocity,  $u_r$

at different axial locations,  $z$ . For  $z > 0.6L$ , where temperature gradients are small,  $u_r$  becomes independent of  $z$  and tends to the function  $V(r)$  in (22). In figure 11, the left and right-hand sides of (25) are compared, with the left hand side evaluated at different  $z$ . We find that the two quantities are equal in the range  $0.6 < z/L < 1.0$  that lies outside the density perturbation, consistent with the discussion at the end of Section 3.2.

## 5 Conclusion

In this study, we have looked at the fundamental problem of the evolution of a buoyant blob of fluid subject to a vertical magnetic field. Contrary to what is found for the evolution of a blob in an infinite domain, both the vorticity and linear momentum of a fluid blob in a finite domain are constrained by the magnetic field. The final state of the blob is determined by two competing timescales: that for the attainment of a quasi-steady state, and that for the emergence of nonlinear advection of vorticity. The relative magnitudes of these timescales are dependent on the strength of the magnetic field as well as the aspect ratio of the fluid domain. Under a strong-enough magnetic field, the quasi-steady timescale controls the dynamics of the blob. In large fluid domains and weak magnetic fields, the nonlinear timescale takes control, and the subsequent behaviour would be similar to what we find in classical (nonmagnetic) flows.

The author's work is sponsored by Research Fellowship from the Leverhulme Trust, U.K.

## References

- [1] R. Moreau, Magnetohydrodynamics, Kluwer Acad. Publ., 1990.

- [2] L. Fraenkel, *J. Fluid Mech.* 7 (1959) 81.
- [3] B. Sreenivasan, P. A. Davidson, J. Etay, *Phys. Fluids* 17 (2005) 117101.
- [4] P. A. Davidson, *J. Fluid Mech.* 299 (1995) 153.
- [5] B. Sreenivasan, T. Alboussière, *Eur.J.Mech. B-Fluids.* 19 (2000) 403.
- [6] B. Sreenivasan, T. Alboussière, *J. Fluid Mech.* 464 (2002) 287.
- [7] A. Pumir, E. D. Siggia, *Phys. Fluids A* 4 (1992) 1472.
- [8] W. E. C.-W. Shu, *Phys. Fluids* 6 (1994) 49.
- [9] P. A. Davidson, B. Sreenivasan, A. J. Aspden, *Phys. Rev. E* 75 (2007) 026304.
- [10] H. K. Moffatt, in: J. Lielpeteris, R. Moreau (Eds.), *Liquid Metal Magnetohydrodynamics*, Kluwer Acad. Publ., Dordrecht, 1989,p.403.
- [11] H. K. Moffatt, D. E. Loper, *Geophys. J. Int.* 117 (1994) 394.
- [12] J. Shercliff, *A Textbook of Magnetohydrodynamics*, Pergamon Press, 1965.
- [13] G. K. Batchelor, *An Introduction to Fluid Mechanics*, Cambridge, 1967.
- [14] J. Sommeria, R. Moreau, *J. Fluid Mech.* 118 (1982) 507.

No.	$\tau$	$L$	$u(t \sim \tau)$	$N_0$	$t_{nl} (theor)$	$t_{nl} (comp)$
1	$10^{-3}$	$20\delta$	$1.2 \times 10^{-5}$	$8.33 \times 10^5$	$8854\tau$	—
2	$4 \times 10^{-3}$	$20\delta$	$4.8 \times 10^{-5}$	$5.208 \times 10^4$	$1395\tau$	$1000\tau$
3	$10^{-2}$	$20\delta$	$1.2 \times 10^{-4}$	8333.3	$411\tau$	$300\tau$
4	$10^{-1}$	$20\delta$	$1.2 \times 10^{-3}$	83.33	$19\tau$	$20\tau$

Table 1: Summary of the buoyant blob regimes considered in this study. The comparison between theoretical estimates and computed values of  $t_{nl}$  is given where linear–nonlinear transitions are found.

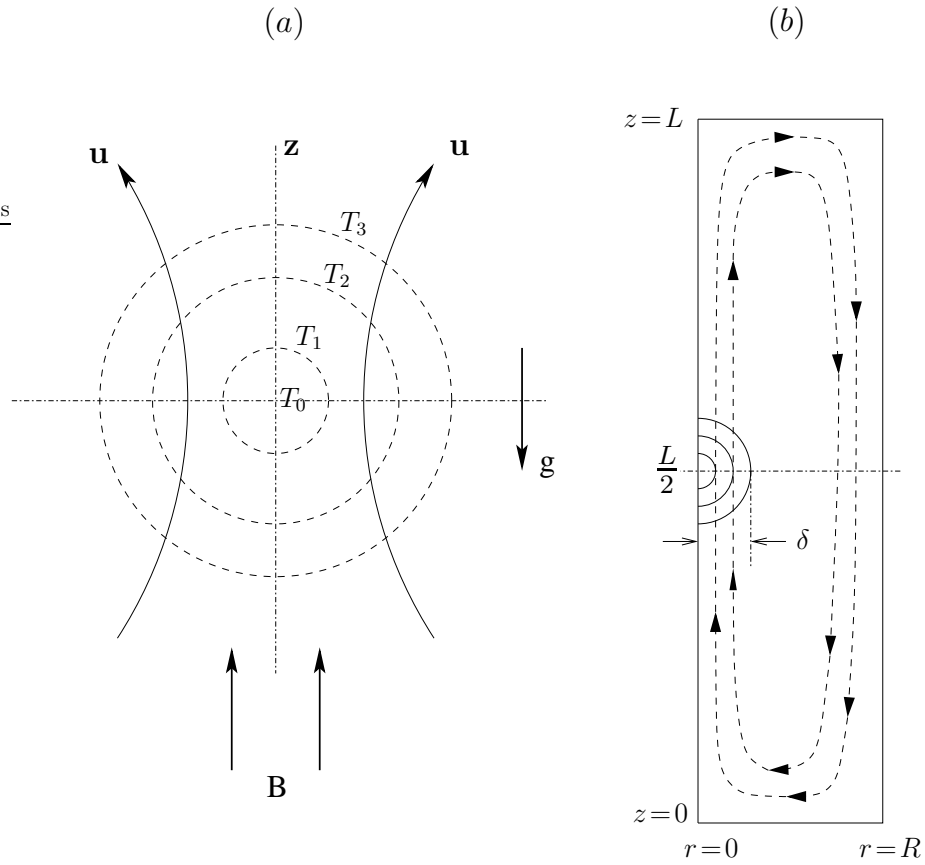


Figure 1: (a) A hot fluid blob of maximum temperature  $T_0$  sits in a vertical magnetic field,  $\mathbf{B}$ . The radial temperature gradients generate the poloidal velocity field  $\mathbf{u}$  which, in turn, is damped by the magnetic field. (b) The model problem of a blob of radius  $\delta$  in a confined domain of height  $L$  and radius  $R$ . Only one half of the domain is shown.

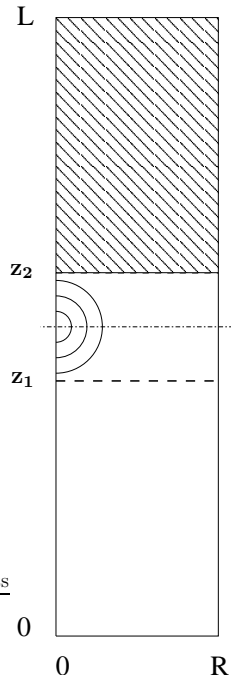


Figure 2: When  $N \gg 1$ , the temperature gradients are confined to the region between the sections  $z_1$  and  $z_2$ . These gradients determine the streamfunction in the hatched region.

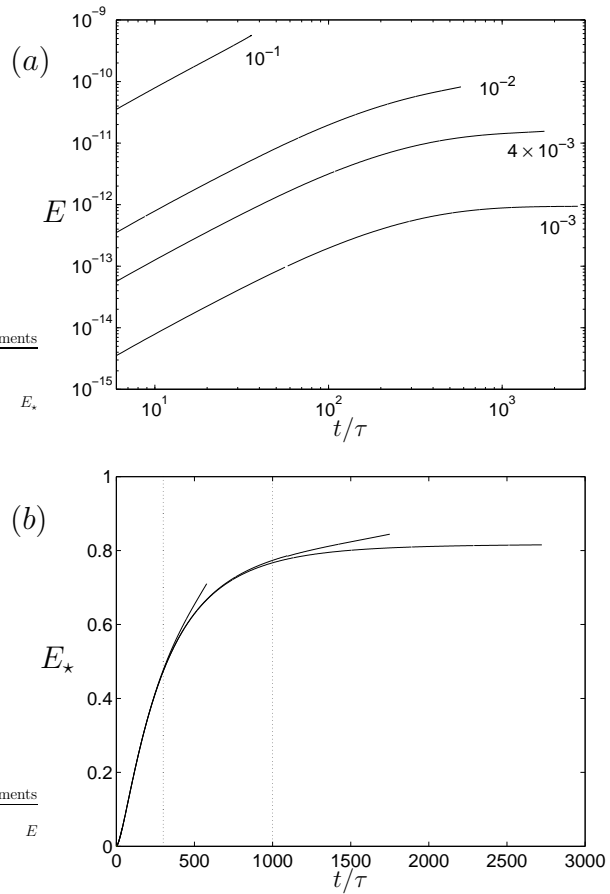


Figure 3: (a) Logarithmic plot of global kinetic energy,  $E$ , with values of  $\tau$  shown near each curve. (b) Global kinetic energy, normalized by the scaling in (30). The vertical lines correspond to the times when self-similarity breaks down, indicating a transition to the nonlinear phase of evolution.

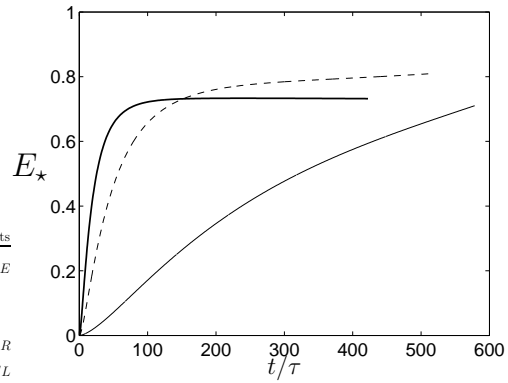


Figure 4: Global kinetic energy, normalized by the scaling in (30), for  $N_0 = 8333.3$ . The different domain geometries studied are (a)  $5\delta \times 5\delta$  (thick solid line); (b)  $8\delta \times 5\delta$  (dashed line) and (c)  $20\delta \times 5\delta$  (thin solid line).

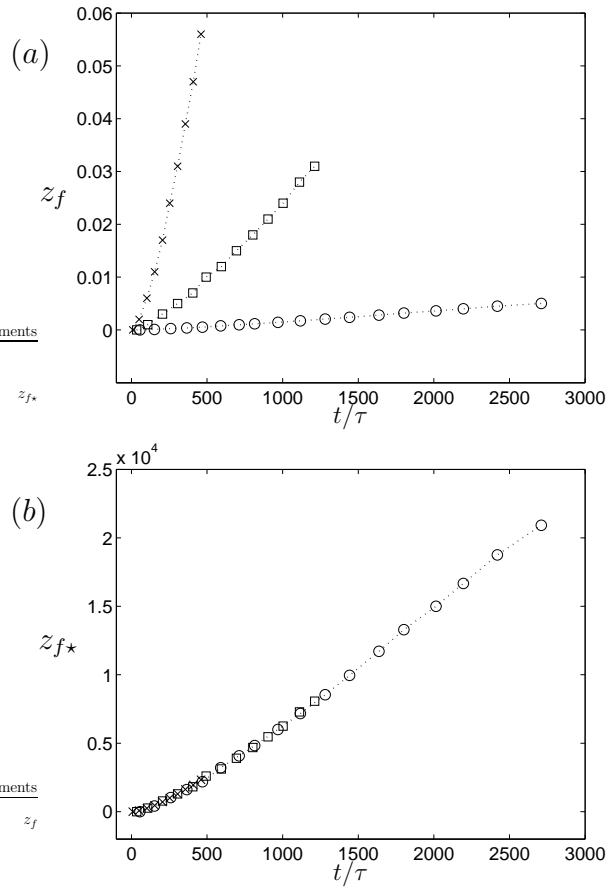


Figure 5: (a) Axial displacement of the blob,  $z_f$ , for  $N_0 = 8.3 \times 10^5$  (circles),  $N_0 = 5.2 \times 10^4$  (squares) and  $N_0 = 8333$  (crosses). (b) Axial displacement normalized by the scaling in (31).

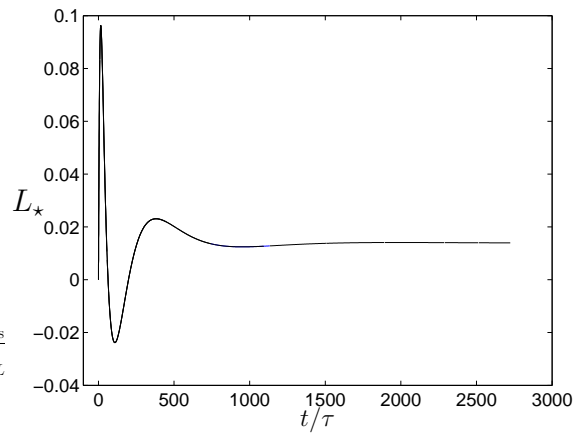


Figure 6: Global Linear momentum normalized by the scaling in (32). The curves for  $N_0 = 8.3 \times 10^5$ ,  $N_0 = 5.2 \times 10^4$  and  $N_0 = 8333$  collapse to a single curve.

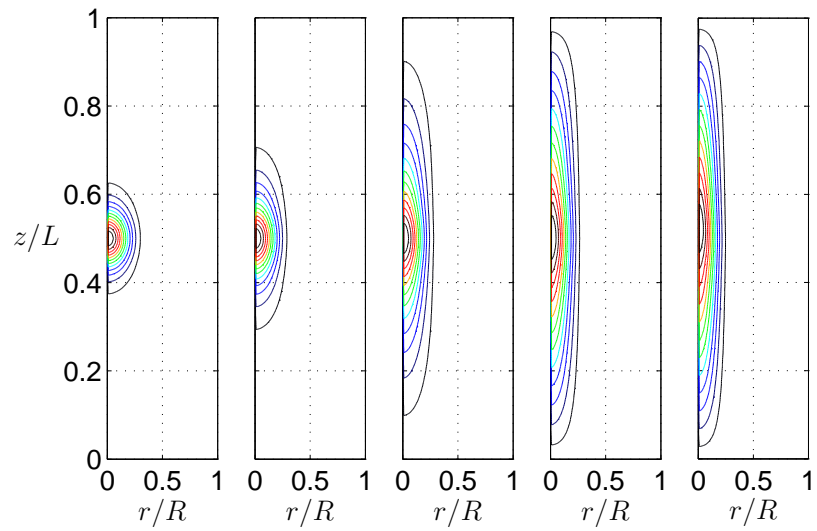


Figure 7: Contour plots of  $\omega_\theta/r$  for  $N_0 = 8.33 \times 10^5$ , at times  $t = 5\tau$ ,  $18\tau$ ,  $100\tau$ ,  $300\tau$  and  $500\tau$ .

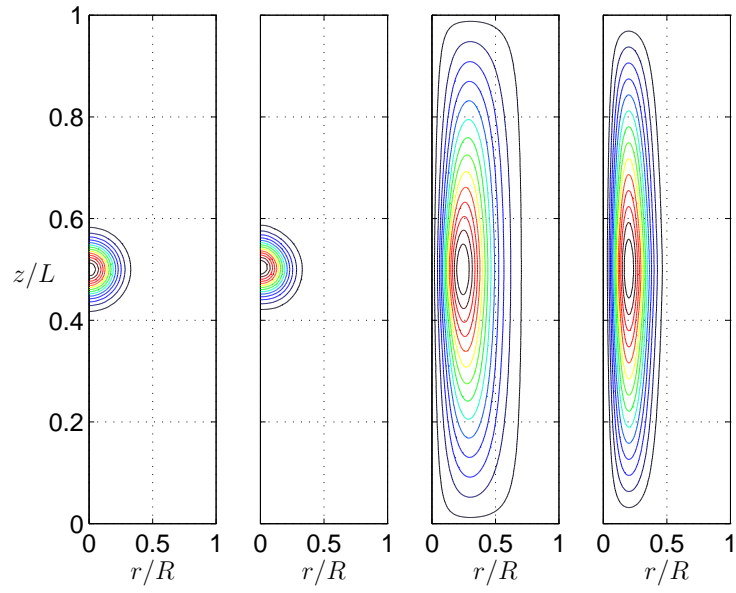


Figure 8: Contour plots for the case  $N_0 = 8.33 \times 10^5$ , shown from left to right in this order: temperature,  $T$ , at time  $t = 100\tau$ ;  $T$  at  $t = 2500\tau$ ; streamfunction,  $\psi$ , at  $t = 100\tau$ ;  $\psi$  at  $t = 2500\tau$ .

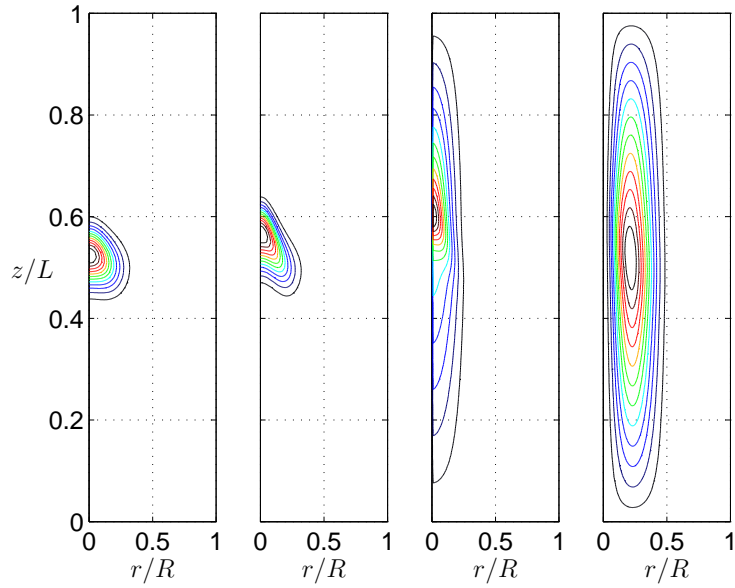


Figure 9: Contour plots for  $N_0 = 8333.3$ , shown from left to right:  $T$  at time  $t = 350\tau$ ;  $T$  at  $t = 600\tau$ ;  $\omega_\theta/r$  at  $t = 600\tau$ ;  $\psi$  at  $t = 600\tau$ .

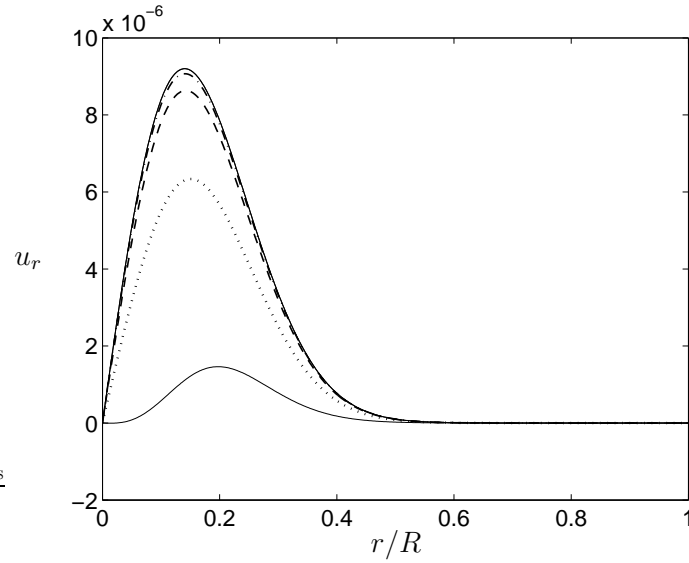


Figure 10: Radial variation of  $u_r$  at different axial locations, for  $N_0 = 8.33 \times 10^5$  and  $t = 2700\tau$  (in the quasi-steady state). The curves from bottom to top are for  $z/L = 0.52$  (solid line), 0.55 (dotted), 0.58 (dashed), 0.60 (dashed-dotted), 0.65 & 0.70 (superposed solid lines).

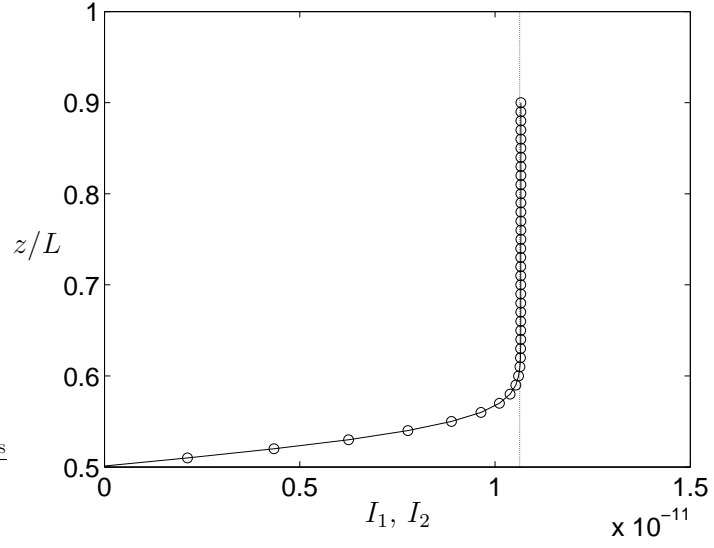


Figure 11: Comparison of the left hand and right hand sides of (25), given by  $I_1$  and  $I_2$  respectively, for  $N_0 = 8.33 \times 10^5$  at  $t = 2700\tau$  (quasi-steady state). The constant value of  $I_2$  is given by the thin vertical line.